Electronic Supplementary Information (ESI)

2D nanoarchitectonics for exfoliated nanosheets: Tailoring surface roughness of thin-film coatings

Hisafumi Sudo,[a] Yuta Nishina,[b,c] Hiroaki Imai,[a] Yuya Oaki*,[a]

[a] Department of Applied Chemistry, Faculty of Science and Technology, Keio University, 3-14-1 Hiyoshi, Kohoku-ku, Yokohama 223-8522, Japan

[b] Research Institute for Interdisciplinary Science, Okayama University, 3-1-1 Tsushima-naka, Kita-ku, Okayama 700-8530, Japan

[c] Institute for Aqua Regeneration, Shinshu University, Nagano 380-8553, Japan

E-mail: oakiyuya@applc.keio.ac.jp

Contents

Experimental methods

Synthesis of the layered composites. Two types of pristine layered titanates were prepared by solid-state syntheses at 800 °C (LT) and 1100 °C (HT) as follows.[63,64] A commercial clay mineral (Kunimine, Kunipia F, montmorillonite) and graphene oxide (GO, NiSiNa Material) were used as purchased without further purification. A guest, tetradecylamine ($C_{14}H_{29}NH_2$, TCI 96.0 %), was intercalated in these host layers by the following procedure.

C_{14}-TiO_2 (LT): The mixture of titanium dioxide nanoparticles (TiO_2, Ishihara Sangyo, ST-01) and cesium carbonate (Cs_2CO_3, Kanto 98.0 %) by the weight ratio 5.2:1.0 was calcined at 500 °C for 1 h under air atmosphere.[63] After mixing in a mortar again, the mixture was sintered at 800 °C for 20 h under air atmosphere. The resultant cesium titanate (Cs-TiO_2) was immersed in 1 mol dm^{-3} hydrochloric acid (HCl). The colloidal dispersion at the concentration 10 g dm^{-3} was maintained at room temperature for one day. The supernatant was changed to the fresh HCl. This ion-exchange from cesium ion to proton was carried out three times, total three days. The precipitate was rinsed with purified water using centrifugation at 3000 rpm for 10 min. After washing several times, the precipitate was collected and dried at room temperature. The resultant protonated titanate (H-TiO_2 (LT), 0.4 g) was added to the aqueous dispersion (100 cm^3) of $C_{14}H_{29}NH_2$ (0.35 g) for 10 days. The precipitate was rinsed with ethanol and tetrahydrofuran (THF) using centrifugation at 3000 rpm for 10 min three times. Then, the collected precipitate of $C_{14}H_{29}NH_2$-intercalated titanate (C_{14}-TiO_2 (LT)) was dried at room temperature.

C_{14}-TiO_2 (HT): The potassium- and lithium-intercalated layered titanate ((K, Li)-TiO_2) was synthesized from the mixture of titanium dioxide nanoparticles (TiO_2, Ishihara Sangyo, ST-01), potassium carbonate (K_2CO_3, Fujifilm-Wako 99.5 %), and lithium carbonate (Li_2CO_3, Kanto 99.0 %) with the weight ratio 100:40:9.2 at 1100 °C for 5 h under air atmosphere.[64] The interlayer cations were exchanged to proton with the immersion of 3 g (K, Li)-TiO_2 in 50 cm^3 purified water with adding 3 cm^3 sulfuric acid (H_2SO_4, Kanto 96.0 %) for 4 h under stirring. The ion-exchange to organic guest was carried out by the same procedure as that for C_{14}-TiO_2 (LT), except that the weight of $C_{14}H_{29}NH_2$ was 0.70 g. In this manner, the $C_{14}H_{29}NH_2$-intercalated titanate (C_{14}-TiO_2 (HT)) was obtained.

C_{14}-GO: The ion-exchange process was modified based on a previous report.[61] GO powder (50 mg) was added to the dispersion liquid containing 500 mg $C_{14}H_{29}NH_2$ in 80 cm^3 purified water. The suspension was maintained at 60 °C for 5 h under stirring. The precipitate was filtered and washed with ethanol and THF. The resultant powder was dried under vacuum at room temperature.

C_{14}-clay: The ion-exchange process was modified based on a previous report.[62] The commercial clay (2.60 g, 2.82 meq CEC) was immersed in 200 cm^3 purified water to promote the swelling at 60 °C for several hours. An aqueous solution containing 2.8 mmol $C_{14}H_{29}NH_2$ and 2.8 mmol HCl was prepared with 20 cm^3 purified water. The solution containing the guest was added to the clay dispersion liquid. The mixture was maintained at 60 °C for 5 h under stirring. The precipitate was rinsed with water and ethanol using centrifugation 3000 rpm for 10 min twice and then rinsed with ethanol and THF using centrifugation 3000 rpm for 10 min twice. The resultant powder was dried at 60 °C.

Exfoliation of the layered composites. The layered composites were exfoliated into the nanosheets. The amine-intercalated layered precursors (0.1 g) were dispersed in 20 cm^3 of benzyl alcohol. The dispersion liquid was sonicated with the ultrasound irradiation (Branson Sonifier set at level 5) for 15 min. The bulk and unexfoliated precipitates were removed using the following filters and sieves: PTFE filter with the pore size 2 μm for C_{14}-TiO_2 (LT) and C_{14}-clay and stainless sieve with the pore size 45 μm for C_{14}-TiO_2 (HT). Such filtration was not performed for C_{14}-GO. The dispersion liquid after the filtration was used for the characterization of the size using DLS. The exfoliated nanosheets were collected using a filter with the pore size 0.1 μm and dried under vacuum for several day.

Redispersion of the nanosheets and their coating on substrates. For spray coating, 45 mg of the exfoliated nanosheet powder was added to 3 cm^3 of methanol for C_{14}-TiO_2 (LT), C_{14}-TiO_2 (HT), and C_{14}-clay or 9 cm^3 of toluene for C_{14}-GO. The vessel was sonicated in a sonic bath to ensure the redispersion for 30 min. The dispersion liquid poured into a spray bottle. Cleaned glass substrates 2.5 cm × 2.5 cm were set on a table. The spraying was repeated with the interval of 30–60 s to use all the coating solution. The superhydrophobic surfaces were prepared by repeating the coating cycle several times. The primary layer was prepared by spraying the toluene dispersion liquid (9 cm^3) containing 45 mg C_{14}-GO nanosheets two times. Then, the methanol dispersion liquid (3 cm^3) containing 33.8 mg C_{14}-TiO_2 (LT) and 11.3 mg r-GO (TCI) nanosheets was sprayed on the primary coating after drying two times.

The same dispersion liquid was used for drop casting. Cleaned silicon substrates were set on a temperature-controlled stage. The temperature was set at 100 °C for methanol and 150 °C for toluene. The temperature was higher than boiling point by ca. 40 K. After the substrate was heated at a certain temperature for 1 min, 10 mm^3 of the dispersion liquid was dropped on the

substrate twice.

The same dispersion liquid was used for spin and dip coatings. About 100 mm^3 of the dispersion liquid was dropped on a glass substrate, the substrate was rotated at 350 rpm 5 s and 1000 rpm for 40 s at room temperature. The dip-coating was performed by immersing the substrate for 10 s and then withdrawing perpendicularly at the rate ca. 10 mm s^{-1}.

Structural characterization. The crystal structure and interlayer distance of the layered materials were characterized using XRD (Bruker D8 Advance) with Cu-Kα radiation. The composition of the interlayer guest was analyzed using TG-DTA (SII TG/DTA 7200) under air atmosphere with heating rate 10 K min^{-1}. The detailed calculation method was described in the text in Fig. S1. The morphologies of the precursor layered materials and coatings were observed using SEM (FEI Inspect F50 and JEOL JSM7100F) operated at 5 kV. The SE and BSE images were observed at 1.5 kV on the cross section and 9 kV on the surface (Zeiss Merlin VP Compact). The EDX spectra were obtained at 10 kV. The sample was coated with amorphous osmium to ensure the conductivity. The lateral size and thickness of the exfoliated nanosheets were measured using TEM (FEI Tecnai G2) operated at 200 kV and AFM (Shimadzu SPM 9700HT), respectively. The dispersion liquid was dropped on a copper mesh supported with collodion membrane for TEM and a cleaned silicon substrate for AFM. The particle size distribution was measured using DLS (Ohtsuka Electronics ELSZ-2000ZS). The surface roughness of the nanosheet coatings was observed using laser microscopy (Keyence VK-X1000). The magnification was set to ×50 for spray coating and ×150 for drop casting. Water contact angle (θ_w) was measured by dropping 8 or 3 mm^3 of water on the surface using a syringe (Kyowa Interface DropMaster). The measurement was carried out on three different positions. The both left and right sides of the droplet were used for the measurement. The average value was calculated by these total six θ_w values.

Structural analyses of the precursor layered composites

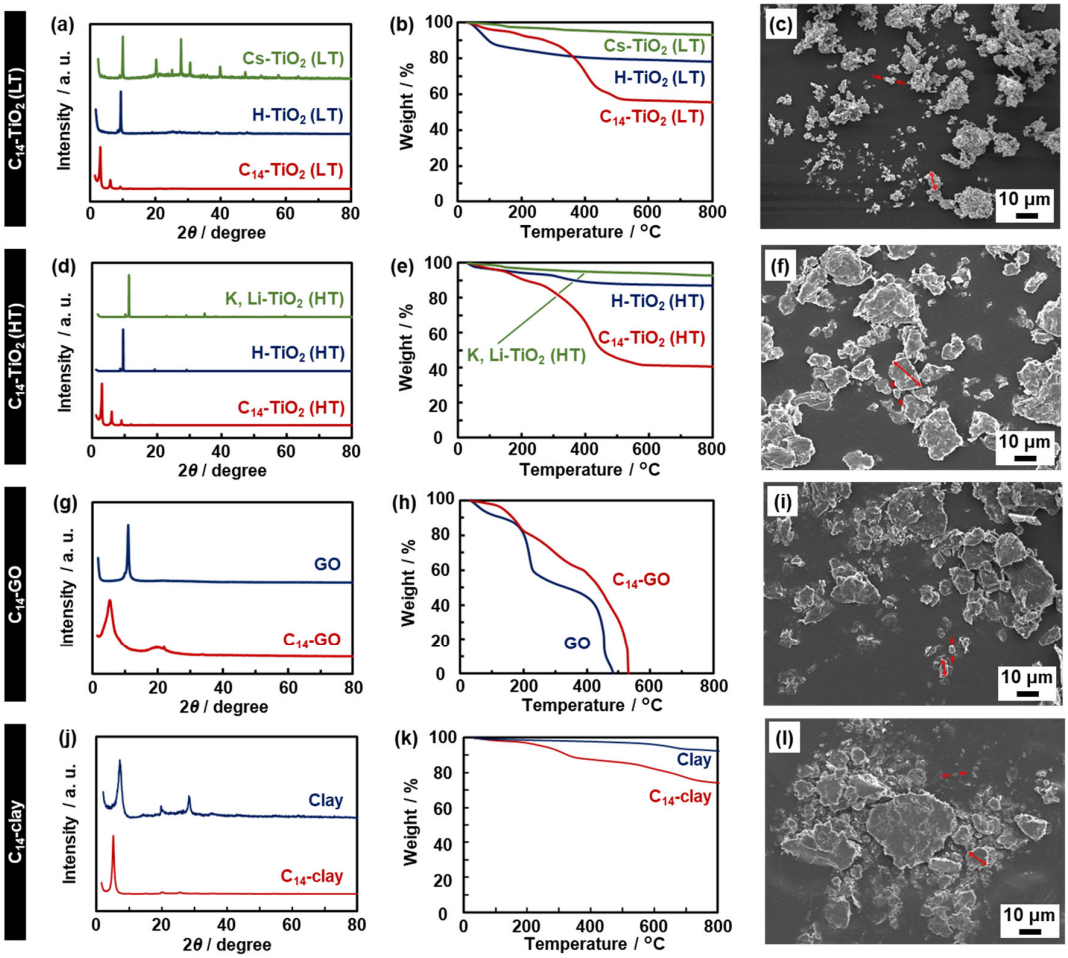

Fig. S1. XRD patterns (a,d,g,j), TG curves (b,e,h,k), and SEM images (c,f,i,l) of C_{14}-TiO_2 (LT), C_{14}-TiO_2 (HT), C_{14}-GO, and C_{14}-clay and their pristine layered compounds.

The results were summarized in Table 1 in the main text. The XRD patterns showed the peaks characteristic of the layered structures (Fig. S1a,d,g,j). The interlayer distance (d_0 / nm) was calculated from the peaks in the low-angle region The composition was calculated based on the TG curves by the following methods (Fig. S1b,e,h,k).[55] The lateral size was estimated from the multiple samples in a number of SEM images (Fig. S1c,f,i,l).

Here the proton-intercalated layered titanate was used as a model to describe the calculation method of the composition in Table 1, except C_{14}-GO. If a part of proton in $H_{0.7}Ti_{1.825}\square_{0.175}O_4 \cdot H_2O$ is exchanged to the guest molecule (x) with hydration (y), the composition is represented by $H_{0.7-x}(Guest)_xTi_{1.825}\square_{0.175}O_4 \cdot yH_2O$. In the TG curve, the weight losses corresponding to water lower than 200 °C and guest in the range of 200–800 °C are defined as w_1 and w_2, respectively. The molecular weights of the guest and remaining inorganic

compounds after combustion are set as M_1 and M_2, respectively. These x, y, M_1, M_2, w_1, and w_2 have the following relationships (Eqs. S1 and S2).

$$(M_1x + 18y + M_2) \times \frac{w_1}{100} = 18y \ldots \text{(Eq. S1)}$$

$$\frac{18y}{M_1x} = \frac{w_1}{w_2} \ldots \text{(Eq. S2)}$$

Then, x and y are calculated from the following two equations (Eqs. S3 and S4).

$$x = \frac{w_2M_2}{(100-w_1-w_2)M_1} \ldots \text{(Eq. S3)}$$

$$y = \frac{w_1}{18w_2}M_1 \times \frac{w_2M_2}{(100-w_1-w_2)M_1} = \frac{w_1M_2}{18(100-w_1-w_2)} \ldots \text{(Eq. S4)}$$

The composition of C_{14}-GO was calculated by the data of CHN elemental analysis. The weight ratio of C, H, and N are summarized in Table S1. The others were regarded as the weight of O. Based on the results, the composition of the intercalated C_{14}-NH_2 was calculated from the increment of the average weight of N.

Table S1. Elemental analysis of pristine GO and C_{14}-GO.

	GO				C_{14}-GO			
Wt %	C	H	N	Others	C	H	N	Others
[a](i)	46.0	3.00	0.10	50.9	68.7	7.44	3.01	20.8
[a](ii)	46.4	2.95	0.11	50.5	68.2	7.39	3.00	21.4
[a](iii)	46.0	3.03	0.13	50.8	68.2	7.32	2.97	21.5
Average	46.2	2.99	0.11	50.7	68.4	7.38	2.99	21.3

[a] The measurement was carried out three times to ensure the reproducibility.

DLS analysis

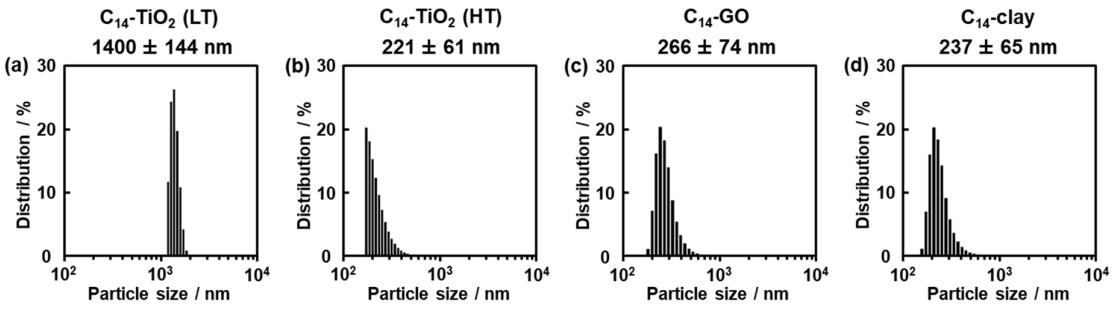

Fig. S2. Particle-size distribution of the C_{14}-TiO_2 (LT) (a), C_{14}-TiO_2 (HT) (b), C_{14}-GO (c), and C_{14}-clay (d) nanosheets exfoliated and dispersed in benzyl alcohol.

The dispersion state of the nanosheets was studied using DLS. The average particle size is not accurate because of the anisotropic morphology of the nanosheets. In our previous works, DLS was used to rough and high-throughput estimation of the size and dispersion state.[54,58] As the DLS chart showed the single peak (Fig. S2), the homogenous dispersion was achieved without strong aggregation. When the additional peaks appear in the larger particle-size region, the aggregates are observed on the TEM images.[54,58]

Cross-sectional SEM images

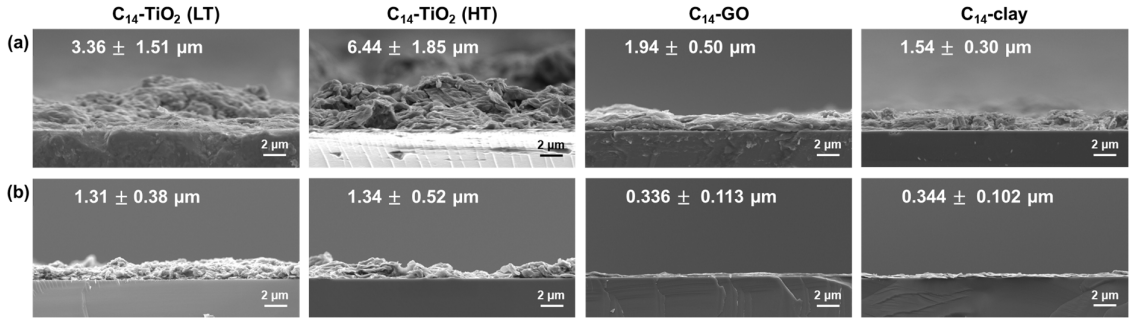

Fig. S3. Typical cross-sectional SEM images with the average thickness of the spray-coated (a) and drop-casted films (b).

The average thickness was estimated from the SEM images in Fig. S3 and additional ones. The thickness was measured on 50 points in each image using ImageJ software. The measurement was carried out on three images including total 150 points. The average and standard deviation were calculated based on these data.

Surface modification with C_{14}-NH_2

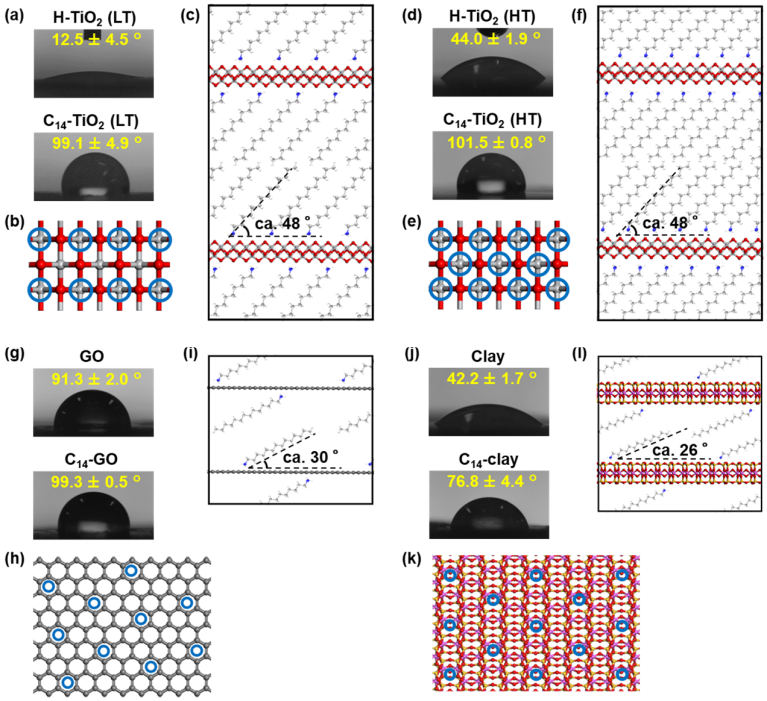

Fig. S4. Surface modification with C_{14}-NH_2 for C_{14}-TiO_2 (LT) (a–c), C_{14}-TiO_2 (HT) (d–f), C_{14}-GO (g–i), and C_{14}-clay (j–l). (a,d,g,j) θ_w of the pristine layered compounds (upper) and composites with the intercalation of C_{14}-NH_2 (lower). (b,e,h,k) Surface planar view of each layer representing the estimated graft site of C_{14}-NH_2 by the blue circle. (c,f,i,l) Cross-sectional view of each layered composite.

The samples with the flat surfaces were prepared by pelletizing each powdered sample using an oil hydraulic press at 10 ton for 1 min. θ_w increased after the intercalation of C_{14}-NH_2 (upper and lower panels in Fig. S4a,d,g,j). The differences in the increment of θ_w originate from the graft density of the long alkyl chains on the layer surface.

The graft density was estimated from the ratio of the guest to the host in Table 1. The structural models of the layer were constructed using a commercial software (Biovia, Materials Studio). The following CIF files were used for preparation of the structural models: 1568984 for C_{14}-TiO_2 (LT) and C_{14}-TiO_2 (HT), 9000046 for C_{14}-GO, and 9002779 for C_{14}-clay. Based on these structural models, the calculated graft density is summarized in Table 3.

Angle independency of the structural color

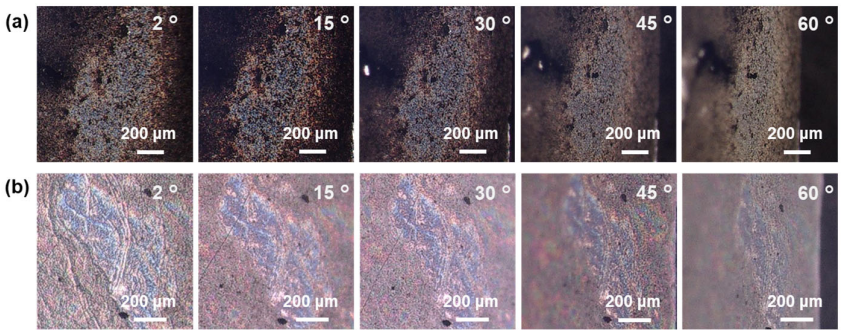

Fig. S5. Optical microscopy images of the C_{14}-GO (a) and C_{14}-clay (b) drop-casted film on silicon substrate with changes in the incident angle of light as described in the image.

When the incident angle of the light source was changed, the color change was not observed. If the coating has the flat surface without microscopic unevenness, the structural color varies with changes in the incident angle.[59] The uneven surface of the coating directs the angle independency.

Morphologies of the spin-coated films

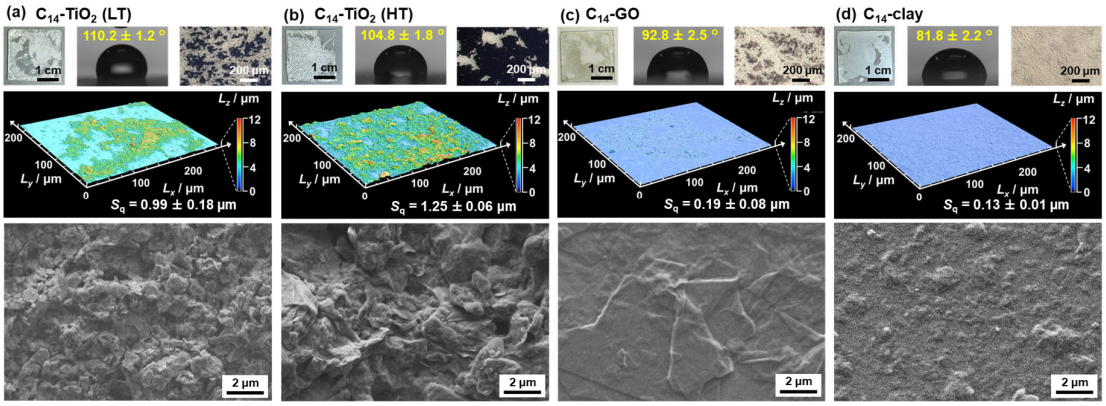

Fig. S6. Macroscopic photographs (top left), water contact angle (top middle), optical microscopy images (top right), LM images (middle), and SEM images (bottom) of the spin-coated C_{14}-TiO_2 (LT) (a), C_{14}-TiO_2 (HT) (b), C_{14}-GO (c), and C_{14}-clay (d) nanosheets on glass substrates. The dispersion medium was methanol for C_{14}-TiO_2 (LT), C_{14}-TiO_2 (HT), and C_{14}-clay and toluene for C_{14}-GO.

The rough and flat surfaces similar to those by spraying were prepared on glass slides. However, the uncoated area was observed macroscopically on the photograph and optical microscopy images (top left and right images).

Morphologies of the dip-coated films

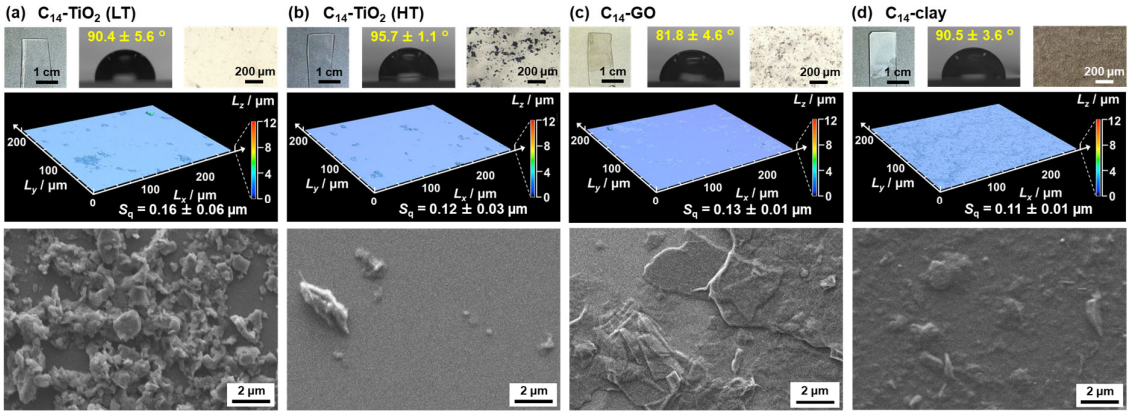

Fig. S7. Macroscopic photographs (top left), water contact angle (top middle), optical microscopy images (top right), LM images (middle), and SEM images (bottom) of the dip-coated C_{14}-TiO_2 (LT) (a), C_{14}-TiO_2 (HT) (b), C_{14}-GO (c), and C_{14}-clay (d) nanosheets on glass substrates. The dispersion medium was methanol for C_{14}-TiO_2 (LT), C_{14}-TiO_2 (HT), and C_{14}-clay and toluene for C_{14}-GO.

The nanosheets were not fully deposited on the substrates. θ_w of the coating was not measured accurately because the bare glass slide was exposed. The viscosity of the dispersion liquid is not sufficient for the dip coating.

TEM image of r-GO

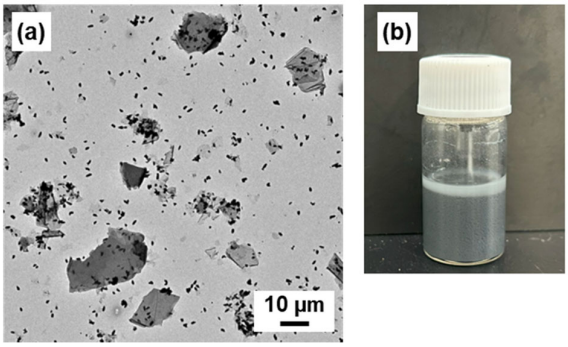

Fig. S8. TEM image of r-GO (a) and photograph of the methanol dispersion liquid containing the C_{14}-TiO_2 (LT) and r-GO nanosheets (b).

The average lateral size of the r-GO was 1.04 ± 1.04 μm (N = 218) (Fig. S8a). As shown in the TEM image, the r-GO had the larger and smaller sheets with the polydispersity.

Both the C_{14}-TiO_2 (LT) and r-GO nanosheets were homogenously dispersed in methanol (Fig. S8b). Based on our previous work,[60] the surface roughness was enhanced by the addition of the more hydrophobic nanosheets with the different size.

Coating in the absence of r-GO

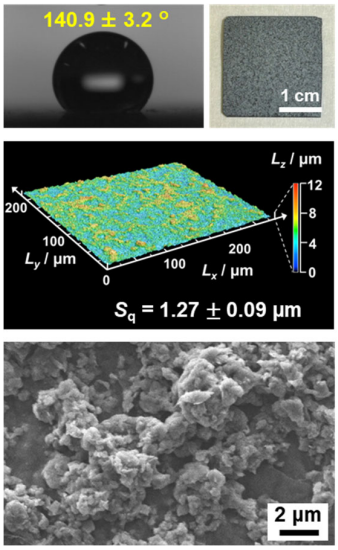

Fig. S9. Water contact angle (top left), macroscopic photographs (top right), LM images (middle), and SEM images (bottom) of the C_{14}-TiO_2 (LT) secondary coating without r-GO on the C_{14}-GO primary coating.

When r-GO was not added to the secondary coating of the C_{14}-TiO_2 (LT) nanosheets, θ_w was lower than 150 °. The addition of r-GO with the different lateral size contributes to enhance the surface roughness.

Effects of r-GO on the surface roughness

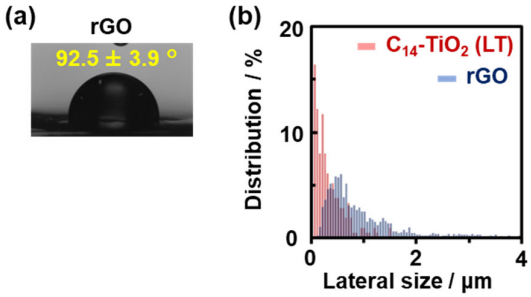

Fig. S10. Effects of r-GO on the enhancement of the surface roughness. (a) θ_w of the pelletized r-GO powder. (b) Lateral size distribution of the mixture of r-GO and C_{14}-TiO_2 (LT).

The flat surface of the r-GO powder was prepared by pelletizing using an oil hydraulic press at 10 ton for 1 min (Fig. S10a). The size distribution in the mixed state of C_{14}-TiO_2 (LT) and r-GO nanosheets was prepared from those of each sample (Fig. S10b). These results imply that the superhydrophobicity is achieved by not only the surface chemistry of r-GO but also the surface roughness derived from the polydispersity of the mixed nanosheets.

Changes in the ratio of r-GO

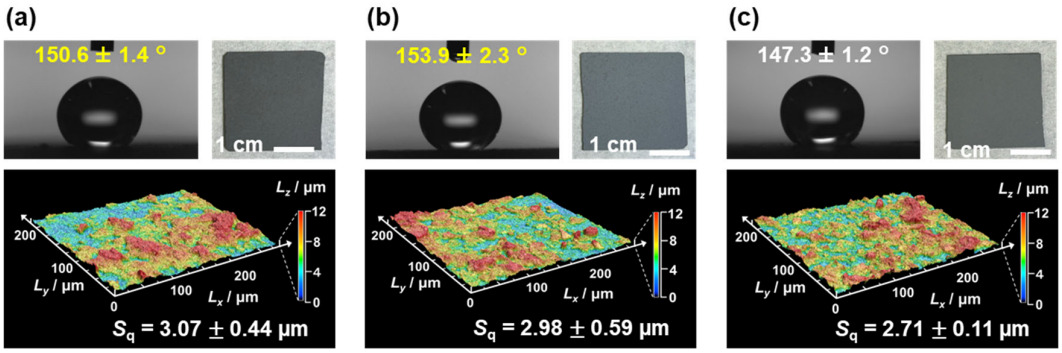

Fig. S11. Water contact angle (top left), macroscopic photographs (top right), and LM images (bottom) of the C_{14}-TiO_2 (LT) coating containing the different weight ratio of C_{14}-TiO_2 (LT) and r-GO. (a) 1:1. (b) 3:1. (c) 5:1.

The superhydrophobic surfaces were achieved on the coatings at the weight ratio 1:1 and 3:1 (Fig. S11a,b). θ_w was lower than 150 for 5:1 (Fig. S11c). LM image with S_q values show that the roughness increased with increasing the ratio of r-GO.